Excited-State Charge Transfer at a Conical Intersection: Effects of an Environment

Irene Burghardt*,† and James T. Hynes*,†,‡

Département de Chimie, Ecole Normale Supérieure, 24 rue Lhomond, F-75231 Paris Cedex 05, France, and Department of Chemistry and Biochemistry, University of Colorado, Boulder, Colorado 80309-0215

Received: December 29, 2005; In Final Form: May 27, 2006

The influence of a polar and polarizable environment on charge transfer processes at a conical intersection (CI) can be described by a diabatic free energy model yielding coupled surfaces as a function of both molecular coordinates and a solvent coordinate. We extend and apply this model for the S_1-S_0 CI in protonated Schiff bases, representing a model for retinal isomerization (*Faraday Discuss.* **2004**, *127*, *395*, 2004). A dielectric continuum description of the solvent is combined with a minimal, two-electron-two-orbital electronic structure model according to Bonačić-Koutecký, Koutecký, and Michl (*Angew. Chem.* **1987**, *26*, 170), which characterizes the charge translocation effects at the CI. The model predicts that the nonequilibrium solvent state resulting from the $S_0 \rightarrow S_1$ Franck−Condon transition can entail the disappearance of the CI, such that solvent motion is necessary to reach the CI seam. The concerted evolution of the intramolecular coordinates and the solvent coordinate is illustrated by an excited-state minimum energy path.

1. Introduction

Conical intersections (CIs) play a key role in the ultrafast decay of photoexcited molecular systems,[1−4] and their importance for biochemical and biological systems has been confirmed over the past decades.[5,6] While the majority of studies to date have addressed CI-induced processes in the gas phase, the influence of an environment on CIs has recently become a topic of intense interest. For example, our study in refs 7−9 is the first explicit investigation of solvent effects on the ground-state reaction path near a CI, and the hybrid quantum mechanical/molecular mechanical (QM/MM) approaches of refs 10−13 provide an avenue to the microscopic description of both ground and excited states in an environment. In ref 14, the reference interaction site model (RISM) is used to locate minimum free energy CIs in solution. Some dynamical aspects relating to high-dimensional model environments and dissipative effects have been addressed, e.g., in refs 15 and 16.

Here we detail, extend and apply a new model approach we have recently introduced[17] to describe an environment's influence on the excited-state processes leading to and occurring at a CI. The model combines an approximate electronic structure description in terms of charge-localized states with a dielectric continuum model for the environment, here taken to be a solvent. As in ref 17, we focus on the application to the excited-state cis−trans isomerization in a small model protonated Schiff base (PSB) in solution. While ref 17 focused on the formulation of a multidimensional free energy model for the system and first considerations of some special cases of nonequilibrium solvation and was restricted to the neighborhood of the CI, the present work (a) includes a detailed account of the basic electronic structure indicating how the important simplification to two valence bond states can be achieved, (b) extends the modeling to include the Franck−Condon region accessed in the excitation of the PSB, and (c) focuses on the perspective of evolving nonequilibrium solvation, characterizing the process in terms of a minimum energy path, as an extension of the approach of ref 18 for the isolated PSB chromophore. A detailed understanding of the process requires quantum-dynamical simulations;[19−22] such simulations are in progress, with initial results reported in refs 23 and 24. The present minimum energy path investigations are nonetheless informative, and they provide first insights on the possible dynamical paths.

The model of ref 17 focuses on CIs involving a charge transfer, so that the dominant features of the chromophore−environment interaction are electrostatic. This applies to protonated Schiff bases (PSBs) like retinal where the S_1-S_0 intersection, which plays a key dynamical role in the cis−trans isomerization of the chromophore, is associated with the translocation of a positive charge.[25] The potential importance of electrostatic effects in the interaction of the retinal chromophore with its environment has been pointed out in refs 26−28. Charge transfer also characterizes, e.g., the earliest events in the photocycle of the photoactive yellow protein, PYP,[10] and the green fluorescent protein, GFP.[29] In the present work, we continue our focus[17] on relatively small PSB systems, for which prior calculations by Robb, Olivucci, and co-workers[18,30−34] and Martínez and co-workers[35,36] assist in constructing the description for the isolated chromophore. Experimental results for retinal and related systems indicating different time scales for the chromophore dynamics in a protein[37−41] and in solution[42−46] suggest that the environmental effect is important.[47,106]

As in ref 17, our model uses an approximate electronic structure description based upon the two-electron two-orbital model by Bonačić-Koutecký, Koutecký, and Michl.[5,6,25,48] Our model is in line with recent theoretical interpretations for the dynamics of retinal and its analogues[18,32,35,36] which provide evidence in favor of a two-state S_1-S_0 model while highlighting the multidimensional character of the initial ultrafast ($\sim$ 100−200 fs) dynamics.[37−39] In particular, the nonadiabatic S_1-S_0 transition takes place at a CI involving skeletal stretching modes besides the torsional mode. We adopt this perspective in the present work, to illustrate an application of the general formulation, in a solution (rather than protein environment) context,

† Département de Chimie, Ecole Normale Supérieure.
‡ Department of Chemistry and Biochemistry, University of Colorado.

10.1021/jp057569c CCC: $33.50
Published on Web 09/19/2006

while acknowledging that the actual molecular mechanism is still under discussion.[31,32,35,36,46,49]

The remainder of this paper is organized as follows. Section 2 briefly reviews the general theoretical formulation for the combined chromophore-environment system in terms of free energy surfaces. Section 3 details an extended two-electron two-orbital model describing the S_1-S_0 dynamics in protonated Schiff bases. In section 4, we address aspects of nonequilibrium solvation and identify features of the minimum energy path. Section 5 summarizes future perspectives and concludes the work.

2. Diabatic Free Energy Model for the S_1-S_0 Conical Intersection in Protonated Schiff Bases

In the present section, we briefly recapitulate some important aspects of ref 17 for the convenience of the reader and to place the developments of the succeeding sections in perspective.

Conical intersections of charge-transfer type—e.g., involving a transition between an ionic and a covalent state—constitute a generic class of CIs in polar double bond systems.[50] Among these, PSBs may be considered a paradigm example, for which S_1-S_0 isomerization can proceed via a CI, for both the C=C and C=N bonds.[5,6,25,48,51] Other examples are the PYP[10] and GFP[29] chromophores whose photocycles are also initiated by isomerization. Different types of excited-state charge-transfer phenomena associated with CIs are discussed, e.g., in refs 52 and 53. While aspects of the succeeding analysis should prove useful in more general contexts, we focus most of the discussion and analysis on the PSB case.

While the above chromophores, and PSBs in particular, exhibit a complicated electronic structure involving various CIs of different types—notably of one-bond flip (OBF) and hula-twist (HT) type[50]—we focus here exclusively on an OBF mechanism involving a twist around a CC double bond. The OBF mechanism is the most common isomerization mechanism for polar double bonds.[50] The CIs in question occur at a twisted geometry of the double bond—often close to 90°[48,35,18,32,34] (according to our model, at exactly 90°,[25,48] see below). According to the two-electron two-orbital model developed by Bonačić-Koutecký, Koutecký, and Michl[25,48] (BKM) in the late 1980s, this CI is associated with a *biradicaloid* structure.

Our analysis for PSBs is based upon an extended version of the BKM model as detailed in section 3. Since we aim to describe the influence of a polar and/or polarizable environment on the intramolecular charge transfer processes associated with the approach to and passage through the CI region, a basis of charge-localized, valence bond (VB) type states is chosen. These provide an example of a diabatic basis of states constructed so as to preserve their charge character in the nonadiabatic coupling region near the CI. While general strategies may be devised to construct such states, we focus here on a simple model which is naturally formulated in terms of appropriate basis functions and highlights the central ideas of the approach.

As explained in ref 17 and developed in detail below, an approximate two-state description can be established based upon the BKM model. Two most relevant configurations can be identified in the basis of p/π-type orbitals localized on adjacent carbons (A and B): a covalent configuration $|AB\rangle$ and an ionic configuration $|B^2\rangle$. These configurations are uncoupled at the 90° twisted geometry. Within the basic model formulation, two types of internal coordinates appear in the role of a coupling mode (twist coordinate θ)—which couples the $|AB\rangle$ and $|B^2\rangle$ configurations away from 90°—and a tuning mode (skeletal stretch coordinate r), respectively.

To describe the PSB−solvent system, the model is augmented by the solvent polarization field interacting with the two VB type solute configurations. Within a dielectric continuum description, the solvent orientational polarization[54] $\mathbf{P}_{or}(\mathbf{x})$ is parametrized by a solvent coordinate z

$$\mathbf{P}_{or}(\mathbf{x}; r,\theta) = z\,\mathbf{P}^{eq}_{or,\mathbf{B}^2}(\mathbf{x}; r,\theta) + (1-z)\,\mathbf{P}^{eq}_{or,\mathbf{AB}}(\mathbf{x}; r,\theta) \quad (1)$$

which describes a general, nonequilibrium $\mathbf{P}_{or}$ state by interpolating between the respective equilibrium states $\mathbf{P}^{eq}_{or,\mathbf{B}^2}$ and $\mathbf{P}^{eq}_{or,\mathbf{AB}}$. This type of collective polarization coordinate has been previously used in models for charge transfer reactions strongly coupled to large amplitude nuclear motion, see, e.g., refs 7 and 55−59.[60] The description of time-evolving $\mathbf{P}_{or}$ nonequilibrium states is a crucial aspect of our model. For example, photoexcitation $S_0 \rightarrow S_1$ leads to a pronounced nonequilibrium situation whose subsequent time evolution reflects the solvent reorganization with respect to the excited-state charge distribution.

Using these elements, the PSB-solvent system can be represented by free energy surfaces of the form[17]

$$\mathbf{G}(r,\theta,z) = \begin{pmatrix} V_{B^2}(r,\theta) + G_s^{B^2}(z; r,\theta) & \tilde{\gamma}(\theta) \\ \tilde{\gamma}(\theta) & V_{AB}(r,\theta) + G_s^{AB}(z; r,\theta) \end{pmatrix} \quad (2)$$

with $\boldsymbol{G}$ a function of the internal coordinates (r,θ) and the solvent coordinate z, which represents an additional degree of freedom within the model. The Vs are the VB state vacuum potentials, with a parametrization in (r,θ) as described in ref 17 and summarized in section 3.3 and in Appendix A, which is adapted to available experimental and ab initio data but is not currently ab initio based. The G_ss are nonequilibrium VB free energies for the solvent in interaction with the VB state charge distributions

$$G_s^{AB}(z; r,\theta) = G_{eq}^{AB}(r,\theta) + \frac{1}{2}k_s(r,\theta)\,z^2$$

$$G_s^{B^2}(z; r,\theta) = G_{eq}^{B^2}(r,\theta) + \frac{1}{2}k_s(r,\theta)\,(1-z)^2 \quad (3)$$

corresponding to "Marcus-like" parabolas displaced along the solvent coordinate z, with the solvent force constant $k_s(r,\theta)$.

The renormalized coupling $\tilde{\gamma}(\theta)$ of eq 2 includes a purely solvent-induced component,[61,62] such that the solvent can have a symmetry-breaking effect. Here we disregard the latter since the dominant environmental influence can be assumed to be of "tuning" (diagonal) type.

Section 3.3 details the conditions for which the model eq 2 is obtained from a more general three-state description (which was not provided in ref 17). Despite its limitations—relating to the approximations in the electronic structure description and the use of a dielectric continuum model for the solvent—the model (i) reproduces the essential electronic structure characteristics identified in the high-level calculations of refs 18 and 30−34 and (ii) allows systematic predictions of static and dynamical (nonequilibrium) environmental effects upon a CI situation.

While a diabatic model for the isomerization process in PSBs has been previously proposed,[20,63] in the present model the roles of the individual intramolecular coordinates differ significantly from those in refs 20 and 63. Furthermore, the present model refers to a diabatic basis exhibiting *localized charge properties*,

which are preserved in the nonadiabatic coupling region. This charge-localized, VB-type, basis is key to including the environment's effects for PSBs.

3. Extended Two-Electron Two-Orbital Model

In this section, we first briefly review the BKM model (which we generalize). The charge characters of the three states involved are then described and we conclude with the reduction to a two-state model.

The two-electron two-orbital BKM model[25,48] explains the occurrence of the S_1-S_0 CI in question by a degeneracy, at a biradicaloid geometry, of covalent ("dot−dot") and ionic ("hole−pair") type configurations. A key model observation is that the electronegativity difference across the double bond, measured by a parameter δ,[25,48] determines whether a CI can actually be found: With increasing δ, the S_1 state is stabilized until an S_1/S_0 degeneracy is met at a threshold value. This value determines the occurrence of a "critically heterosymmetric" biradicaloid structure[25] at the 90° twisted geometry of the double bond.[64] The model thus explains that, while no CI is found for twisted ethylene ($\delta = 0$)—in the absence of asymmetric perturbations as induced, e.g., by pyramidalization—CIs do occur for PSBs at the twisted geometry (possibly as a function of other, symmetric modes).

In PSBs, the relevant electronic configurations are associated with charge distributions corresponding to the positive charge localized on the nitrogen containing moiety for the ground state ("dot−dot" configuration), while the charge is localized on the hydrocarbon moiety for the first excited state ("hole−pair" configuration).[18,25,32,34] Thus, the S_1-S_0 transition gives rise to a charge *translocation*.[25] This image is borne out in recent electronic structure studies of short analogues of the retinal chromophore, by Robb, Olivucci and co-workers[18,30−34] and by Martínez and co-workers.[35,36] The coupling of the environment's polarization field to the charge translocation process is the central interest of the model detailed below.

In the following, we review and extend the BKM model, which in its original form refers specifically to the biradicaloid geometry. We develop a suitable parametrization which takes into account the dependence on the internal coordinates and the external polarization field. With this extension, the model will be shown to yield a suitable diabatic representation for the PSB S_1-S_0 CI.

3.1. Three-State Model. A basis of localized p-orbitals is particularly appropriate for the CC bond isomerization, to characterize the CI occurring at the 90° twisted biradicaloid geometry. Hence, we give preference to this representation as opposed to the more familiar representation in terms of π/π^* orbitals, most appropriate for the planar geometry. The σ bonding framework is not explicitly considered.

We thus refer to the two-electron basis for two p orbitals on neighboring centers (i.e., pπ-type orbitals) with the notation A $\equiv p_A$ and B $\equiv p_B$,

$$\begin{aligned} {}^1|\mathrm{AB}\rangle &= (1/\sqrt{2})\,[\mathrm{A}(1)\mathrm{B}(2) + \mathrm{B}(1)\mathrm{A}(2)]\otimes|\Sigma\rangle \\ {}^1|\mathrm{A}^2\rangle &= [\mathrm{A}(1)\mathrm{A}(2)]\otimes|\Sigma\rangle \\ {}^1|\mathrm{B}^2\rangle &= [\mathrm{B}(1)\mathrm{B}(2)]\otimes|\Sigma\rangle \end{aligned} \tag{4}$$

Since we specifically consider the singlet manifold $|\Sigma\rangle = 1/\sqrt{2}(\alpha_1\beta_2 - \beta_1\alpha_2)$, we will drop the index 1 in the following.[65]

The $|\mathrm{AB}\rangle$ state of eq 4 represents the "dot−dot" configuration mentioned above, with the two electrons assigned to different centers, while the $|\mathrm{A}^2\rangle$ and $|\mathrm{B}^2\rangle$ configurations are of "hole−pair" type, with the two electrons on the same center. The simplest electronic structure model for the PSBs interprets the adiabatic states S_0, S_1, and S_2 as linear combinations of these basis states.

To formulate a model Hamiltonian, it is convenient to use a symmetry-adapted basis involving the ± linear combinations of the hole−pair states $|\mathrm{A}^2\rangle$ and $|\mathrm{B}^2\rangle$,

$$\begin{aligned} {}^1|\mathrm{AB}\rangle &= (1/\sqrt{2})\,[\mathrm{A}(1)\mathrm{B}(2) + \mathrm{B}(1)\mathrm{A}(2)]\otimes|\Sigma\rangle \\ {}^1|Z_+\rangle &= (1/\sqrt{2})\,[\mathrm{A}(1)\mathrm{A}(2) + \mathrm{B}(1)\mathrm{B}(2)]\otimes|\Sigma\rangle \\ {}^1|Z_-\rangle &= (1/\sqrt{2})\,[\mathrm{A}(1)\mathrm{A}(2) - \mathrm{B}(1)\mathrm{B}(2)]\otimes|\Sigma\rangle \end{aligned} \tag{5}$$

where Z denotes "zwitterionic" states. For the two-electron p orbital system at a 90° twisted geometry (D_{2d} symmetry), the states eq 5 are decoupled by symmetry. These may be taken to be the eigenstates of 90° twisted ethylene, in a single-configurational representation of localized p orbitals.

Two types of perturbations may arise which couple the above states.[25,66]

1. The first relates to asymmetric perturbations across the double bond, represented by the parameter δ in eq 6, below. In the present context, perturbations of this type reflect a chemical asymmetry, i.e., the difference in electronegativities across a C═C or C═N double bond. Asymmetric vibrations like the one-sided pyramidalization in ethylene[5,6,25,66−68] (where $\delta = 0$) can play a similar role. Such perturbations lower the symmetry from D_{2d} to C_s.[66,69] The states $|Z_+\rangle$ and $|Z_-\rangle$ are mixed (both of A' symmetry in C_s while of distinct symmetries, A_1 and B_2, in D_{2d}). The effect is to "polarize" the ± linear combinations and obtain states which are closer to the $|\mathrm{A}^2\rangle$ and $|\mathrm{B}^2\rangle$ states of the basis eq 4.

The discussion in BKM centers on perturbations of this type. For PSBs, the state $|Z_-\rangle$—polarized toward $|\mathrm{B}^2\rangle$—is strongly stabilized and may become degenerate with the $|\mathrm{AB}\rangle$ state at a critical value of δ, the critically heterosymmetric case.[70]

2. The second relates to twisting type perturbations, represented by the coupling function $\gamma(\theta)$ in the matrix Hamiltonian eq 6, below. Twisting away from $\theta = 90°$ induces a nonzero overlap and hence π-binding effects between the neighboring centers' p orbitals, while the symmetry is lowered from D_{2d} to D_2. Perturbations of this type mix the states $|\mathrm{AB}\rangle$ and $|Z_+\rangle$ (both of which are of A symmetry in D_2 while they are of A_1 and B_1 symmetry, respectively, in D_{2d}.[66,69]) Since we will be concerned with degeneracies at $\theta = 90°$, and the θ-dependent coupling lifts such degeneracies away from the $\theta = 90°$ twisted geometry, we will hereafter refer to θ as a coupling coordinate, or symmetry-breaking coordinate.[1]

Both types of perturbations are in general strong. Thus, the π-binding effects represented by $\gamma(\theta)$ induce a strong mixing of the $|\mathrm{AB}\rangle$ and $|Z_+\rangle$ states to obtain a π^2 type ground state at the planar geometry. As for the asymmetric perturbations, δ acts such as to effectively polarize the $|Z_-\rangle$ state into the hole−pair state $|\mathrm{B}^2\rangle$, whereas $|Z_+\rangle$ tends toward $|\mathrm{A}^2\rangle$. For the PSBs, the first excited state (S_1) is therefore predominantly of $|\mathrm{B}^2\rangle$ character while S_2 is of $|\mathrm{A}^2\rangle$ character.

A matrix potential reflecting the above two types of perturbations described above can be formulated in the basis $\{|Z_+\rangle, |Z_-\rangle, |\mathrm{AB}\rangle\}$

$$\mathbf{V} = \begin{pmatrix} V_Z(\mathbf{R}) + \Delta_Z(\mathbf{R}) & \delta & \gamma(\mathbf{R}) \\ \delta & V_Z(\mathbf{R}) - \Delta_Z(\mathbf{R}) & 0 \\ \gamma(\mathbf{R}) & 0 & V_{\mathrm{AB}}(\mathbf{R}) \end{pmatrix} \tag{6}$$

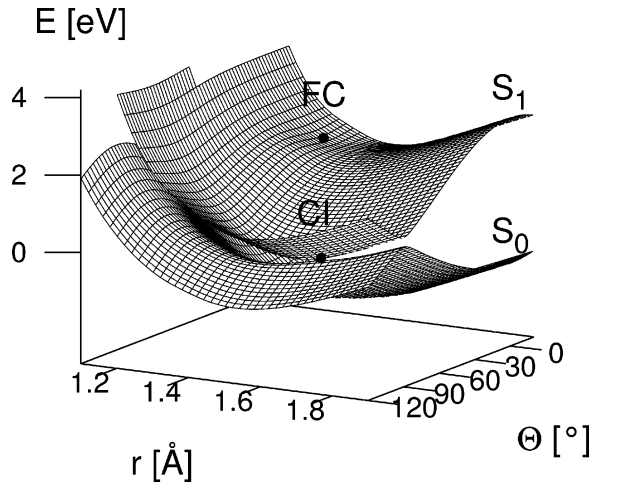

Figure 1. Adiabatic S_0 and S_1 surfaces for the isolated chromophore. The Franck−Condon geometry (FC) and the CI point are marked. The CI is located at ($r_{CI} = 1.59$ Å,$\theta = 90°$).

All matrix elements depend on the internal molecular coordinates, except for the parameter δ. The diabatic potentials for the $|Z_+\rangle$ and $|Z_-\rangle$ states are defined as $V_Z(\mathbf{R}) \pm \Delta_Z(\mathbf{R})$.

The coupling $\gamma(\mathbf{R}) \equiv \gamma(\theta)$ is a function of the twist angle, and vanishes for $\theta = 90°$. As explained above, the $|AB\rangle$ state is then decoupled from the hole−pair states for symmetry reasons, and a CI can therefore arise at the 90° twisted geometry. Such an intersection requires an accidental degeneracy as a function of δ and of the other internal coordinates. We propose below a simple two-mode picture which distinguishes (i) the coupling mode θ and (ii) a tuning (symmetric) mode[1] associated with the CC stretch vibration (or, more generally, a skeletal stretch vibration as in the longer PSBs).

To describe the PSB system-polar environment interaction, the basis $\{|A^2\rangle,|B^2\rangle,|AB\rangle\}$, is most convenient (see section 4). In this basis, the matrix representation eq 6 translates to

$$\mathbf{V} = \begin{pmatrix} V_Z(\mathbf{R}) + \delta & \Delta_Z(\mathbf{R}) & \gamma(\mathbf{R})/\sqrt{2} \\ \Delta_Z(\mathbf{R}) & V_Z(\mathbf{R}) - \delta & \gamma(\mathbf{R})/\sqrt{2} \\ \gamma(\mathbf{R})/\sqrt{2} & \gamma(\mathbf{R})/\sqrt{2} & V_{AB}(\mathbf{R}) \end{pmatrix} \tag{7}$$

In the representations eqs 6 and 7, δ and $\Delta_Z(\mathbf{R})$ exchange their roles as diagonal vs off-diagonal components. As can be inferred from eq 7, the energy difference between the diabatic $|A^2\rangle$ and $|B^2\rangle$ states is 2δ.

Related models referring to both the symmetry-adapted basis in eq 6 and the localized basis in eq 7 have recently been proposed by Tennyson and Murrell[66] and by Domcke, Manthe, and co-workers[68] for ethylene (where $\delta = 0$, but the one-sided pyramidalization takes on the role of an asymmetric perturbation).

3.2. Charge Properties. The representation in eq 7 is most convenient to formulate the interaction with the environment. Indeed we may associate localized, fixed charge distributions with the basis states in eq 4, which can be referred to as valence-bond type states. As noted above, this provides a simple realization of a representation in terms of diabatic states which preserve their charge character in the region of interest for the dynamics. In general, diabatic states as defined, e.g., in refs 1 and 2, are not expected to fulfill this criterion, and a mapping onto an extended space of VB type functions may be required. By contrast, the configurations in eq 4 have the desired properties in the present model.

In the PSBs, the characteristic charge distributions of the states in eq 4 are determined by the presence of a positive excess charge which subtracts an electron from the dot−dot and hole−pair configurations. For the $|AB\rangle$ (dot−dot) state which predominantly represents the ground state of the PSBs, the positive charge is localized on the nitrogen atom. If one thinks of the following partitioning in terms of left and right-hand moieties (see also refs 32 and 35)

$$-C-C=|=C-C=NH_2]^+ \tag{8}$$

where the vertical bar indicates a cut through the C=C double bond, the charge characteristics may be described in a shorthand notation as

$$\begin{array}{ll} |AB\rangle & \boxed{\cdot \;|\; +} \\ |B^2\rangle & \boxed{+ \;|\; \cdot} \\ |A^2\rangle & \boxed{- \;|\; ++} \end{array} \tag{9}$$

From the calculations by Robb, Olivucci, and co-workers[18,32] and Martínez and co-workers,[35] the positive charge is indeed predominantly localized on the nitrogen containing end for the S_0 state, and is predominantly localized on the hydrocarbon end for the S_1 state (A more detailed discussion will be given in section 4.1). Focusing on the $|AB\rangle$ and $|B^2\rangle$ states, which play a central role for the coupled S_1-S_0 dynamics in PSBs, a charge translocation from the hydrocarbon end to the nitrogen end[25] takes place upon the transition between these two states.

Finally, the $|A^2\rangle$ state charge distribution resembles that of the $|AB\rangle$ state in that the positive charge is predominantly localized on the nitrogen-containing moiety, cf. eq 9. From the work by Robb, Olivucci and co-workers[18,32] on the isolated chromophore, the S_0 and S_2 states—predominantly of $|AB\rangle$ and $|A^2\rangle$ character, respectively, near the CI—indeed exhibit very similar charge distributions.

3.3. Reduced Two-State Model. The energetic separation between the hole−pair configurations $|A^2\rangle$ and $|B^2\rangle$—with the $|A^2\rangle$ configuration shifted to high energies—is a key observation for polar double bond systems,[25] which we will use to neglect $|A^2\rangle$ and reduce the model eq 7 to an effective two-state model in the $\{|B^2\rangle,|AB\rangle\}$ basis. However, caution is necessary here, for two reasons.

The first is the very pronounced effect of the coupling $\gamma(\theta)$, which mixes $|AB\rangle$ and $|A^2\rangle$, an effect which is negligible only if the asymmetry parameter δ is substantially larger, $\delta \gg \gamma(\theta)$. This is not necessarily the case for PSBs, whose S_2 adiabatic states (with predominant $|A^2\rangle$ character) are relatively low-lying.[32,39,25] Still, we find for the present model parametrization that if the S_0, S_1, and S_2 states are approximately equidistant at the planar geometry (where the effect of the coupling is maximal, see Figure 2), the admixture of the $|A^2\rangle$ component in the S_0 and S_1 eigenvectors is relatively small (less than 5%). This supports the use of a two-state approximation in the framework of the present discussion.

Second, solvent effects on the state separation have to be taken into account. In particular, the S_1 vs S_2 charge distributions are not stabilized (or destabilized) in the same way by a solvent. Since the S_2 and S_0 charge distributions are similar (see section 3.2), one could envisage a situation where S_2 is stabilized while S_1 is *de*stabilized. This is indeed the situation expected for a Franck−Condon transition, with a solvent initially equilibrated

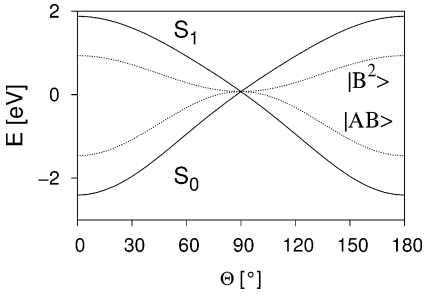

Figure 2. Potential cut through the CI as a function of the torsional angle θ, at $r = r_{CI} = 1.59$ Å. Full lines: adiabatic S_0 and S_1 states, dotted lines: diabatic $|AB\rangle$ and $|B^2\rangle$ states. Note the considerable difference between the diabatic and adiabatic states when moving toward the planar geometry, due to the increasing effect of the diabatic coupling away from $\theta = 90°$.

to S_0. The S_2/S_1 energy difference would then *decrease* compared to the isolated chromophore. A similar effect has recently been observed in model calculations for counterion effects on PSBs.[71]

Despite these caveats, we will employ here a first, approximate analysis based upon a two-state description.[72] The reduced two-state model as derived from eq 7 then takes the final form, with $\mathbf{R} = (r,\theta)$

$$V(r,\theta) = \begin{pmatrix} V_{B^2}(r,\theta) & \frac{1}{\sqrt{2}}\gamma(\theta) \\ \frac{1}{\sqrt{2}}\gamma(\theta) & V_{AB}(r,\theta) \end{pmatrix} \tag{10}$$

with $V_{B^2}(r, \theta) = V_Z(r, \theta) - \delta$. Here, the twist coordinate θ appears in the role of a coupling mode, while r is a tuning mode, as explained above.

In accordance with recent work by Robb, Olivucci, and co-workers,[32] a two-state-two-mode model is indeed the simplest scenario providing a qualitatively correct picture for the S_1-S_0 intersection in the PSBs.[73] According to these authors, the stretching coordinate refers[32] to a framework motion in which CC double bonds lengthen and CC single bonds contract, a feature which ultimately allows the isomerization to proceed. Thus, r is a bond length alternation (BLA) coordinate.[74,75]

The proposed functional form for the potentials as a function of r and θ—based upon sums over analytical Morse type and polynomial terms—has been detailed in ref 17. A brief summary is given in Appendix A. We recall here specifically that the coupling between the $|AB\rangle$ (dot−dot) state and the $|B^2\rangle$ (hole−pair) state is

$$\gamma(\theta) = c_\gamma^{(1)} \cos\theta + c_\gamma^{(3)} \cos^3\theta \tag{11}$$

in accordance with the models developed for ethylene by Domcke, Manthe and co-workers[68] and, for the contribution in $\cos\theta$, by Tennyson and Murrell.[66] The physical origin of the term in $\cos\theta$ is a resonance integral proportional to the overlap between the p orbitals on the neighboring centers;[25,76] the third-order term should be understood as a higher-order correction conforming to the required symmetry. We restrict the present analysis to the term in $\cos\theta$.[77]

While the parametrization of ref 17 is appropriate for the CI region, it does not give an accurate representation at the planar geometry, i.e., the Franck−Condon (FC) region. In particular, the S_1 surface is *bound* in the FC region with respect to the torsional coordinate.[18,30−32] In view of a complete reaction path analysis—crucial for understanding femtosecond to picosecond events—the model Hamiltonian is therefore modified in the present work to account for this feature.

For this purpose, an FC correction term is introduced which makes the diabatic $|B^2\rangle$ potential locally bonding in θ (see also ref 24)

$$V_{FC}(r,\theta) = \frac{k_{FC}}{2}\sin^2\theta\, g_{FC}(r,\theta) \tag{12}$$

with the Gaussian damping function $g_{FC}(r,\theta) = \exp(-(r - r_{FC})^2/\sigma_{r_{FC}})\exp(-\sin^2\theta/\sigma_{\theta_{FC}})$; here $k_{FC} = 0.12$ au, $r_{FC} = 1.39$ Å, $\sigma_{r_{FC}} = 0.07$ Å, and $\sigma_{\theta_{FC}} = 0.62$.[24] The functional form and parametrization were chosen so as to match available ab initio information on the FC region,[18,30−32] while leaving the CI region unaffected.

4. Two-State S_0/S_1 Model for PSBs

We now analyze the predictions of the two-state, three-mode model of eq 2, with the twisting coordinate θ as a coupling mode, the skeletal BLA stretch coordinate r as a tuning mode, and the solvent coordinate z as an additional tuning mode. Solvent effects on the off-diagonal free energy components are neglected at the present level of treatment, i.e., the coupling $\tilde{\gamma}$ of eq 2 is set to $\tilde{\gamma} = \gamma/\sqrt{2}$; see the isolated chromophore Hamiltonian in eq 10. Furthermore, the dependence of the solvent free energies (eq 3) on the internal coordinates is disregarded in this first, qualitative analysis. The solvent force constant is set to $k_s = 2.5$ eV (see Table 1).[17]

We first address the resulting potential surfaces and associated charge distributions for the isolated chromophore (section 4.1), followed by a detailed discussion of the free energy surfaces including the solvent (section 4.2) and the characterization of the S_1 surface by a minimum energy path (section 4.3).

4.1. Isolated Chromophore. Figure 1 shows the adiabatic S_1 and S_0 surfaces for the isolated chromophore, obtained by diagonalizing the matrix eq 10 excluding the solvent contribution. The surfaces feature a CI at $\theta = 90°$ and $r_{CI} = 1.59$ Å, which here coincides with the minimum of the upper adiabatic surface. At the FC geometry, the surface is locally bonding in the θ direction, in accordance with the FC correction eq 12. Note that our previous analysis in ref 17 was restricted to the vicinity of the CI and did not include the FC region; its inclusion in the present description will allow us to explicitly consider the FC region on S_1 in the presence of the solvent.

Figure 2 shows a cut of the potential surface along the torsional coordinate, at a value of the skeletal stretch coordinate corresponding to the intersection point, $r = r_{CI}$. The cut illustrates that while the diabatic and adiabatic surfaces converge toward $\theta = 90°$ (where the diabatic coupling vanishes), they increasingly diverge when moving "back" toward the planar geometry.

The charge distributions in the adiabatic S_0 and S_1 states can be directly inferred from the coefficients in the expansion of the adiabatic wave function in the VB components. Recall that the positive charge is predominantly localized within the nitrogen containing moiety for the $|AB\rangle$ (dot−dot) state, and predominantly localized within the hydrocarbon moiety for the $|B^2\rangle$ (hole−pair) state; see eq 9. For example, at the FC geometry, the S_0 adiabatic state is predominantly of $|AB\rangle$ character while containing a significant admixture of $|B^2\rangle$ character (about 30%), whereas the inverse holds for S_1. This is in qualitative agreement with the experimental observation of a pronounced change in dipole moment in the FC transition.[78]

TABLE 1: Parameter Values for the Potentials as Specified in Appendix A

D_{AB}	5.0 eV
D_{B^2}	4.0 eV
α_{AB}	1.64 Å^{-1}
α_{B^2}	2.05 Å^{-1}
$r_{0,AB}$	1.33 Å
r_{0,B^2}	1.48 Å
Δr_{AB}	0.12 Å
Δr_{B^2}	0.12 Å
c_θ^{AB}	−2.0 eV/rad^2
$c_\theta^{B^2}$	0.5 eV/rad^2
ΔE_{B^2}	0.27 eV
$c_\gamma^{(1)}$	2.5 eV
k_s	2.5 eV

While the VB states mix substantially for geometries away from $\theta = 90°$, they decouple at the CI. Hence, a pronounced *polarization effect* is expected when moving toward the CI from the FC region. This effect is illustrated in Figure 3 for the S_1 adiabatic surface of Figure 1. The figure shows the decomposition of the S_1 eigenvector in terms of its $\{|AB\rangle,|B^2\rangle\}$ components, as a function of the twist angle θ and the tuning coordinate r. A step function-like feature is observed for $\theta = 90°$ along r, reflecting that the adiabatic states correspond to different diabatic branches to the left and right of the CI point. As can be inferred from Figure 3b, the discontinuity is smoothed out away from $\theta = 90°$.

The above observations are in qualitative agreement with the picture described by Robb, Olivucci, and co-workers[18,30−32] and by Martínez and co-workers[35] for different retinal analogues. Since these and other ab initio analyses are based upon an adiabatic perspective, we comment in Appendix B on the relation between the diabatic and adiabatic representations, to facilitate the comparison with our model.

4.2. Free Energy Surfaces Including Solvent: Topological Aspects. The S_0 and S_1 free energy surfaces derived from eq 2 including the solvent contribution are characterized by two tuning modes, r and z, in addition to the coupling mode θ. Hence, the first influence of the solvent is that a *seam* of conical intersections results, i.e., a line in the (r, z) space for $\theta = 90°$, depicted in Figure 4. The fact that the CI seam lies in the subspace of tuning modes is due to the symmetry-allowed nature of the CI under consideration.[79]

The locations (r, z) along the CI seam are determined by the condition $\Delta V(r,\theta = 90°) = \Delta V(r,\theta = 90°) = -\Delta G_s(z)$ for a degeneracy of the two adiabatic (or diabatic) states, given a vanishing coupling ($\theta = 90°$), with $\Delta V(r,\theta) = V_{B^2}(r,\theta) - V_{AB}(r,\theta)$ and the solvent-induced free-energy gap

$$\Delta G_s(z) = G_s^{B^2}(z) - G_s^{AB}(z) = k_s\left(\frac{1}{2} - z\right) \qquad (13)$$

The required degeneracy at the CI seam is achieved by matching the respective energy gaps induced by the two tuning coordinates.

Note the location of the minimum (free) energy conical intersection (MECI) in Figure 4 for the seam at ($r = 1.54$ Å, $z = 0.55$). The slight departure of the MECI from the midpoint $z = 0.5$ follows from an analytic analysis of the model, detailed in Appendix C. Since the solvent contributions to the diabatic state energies are very similar for $z_{MECI} = 0.55$—and, concomitantly, $\Delta G_s(z_{MECI})$ is very small—the location of the MECI in r is very similar to the CI location in the isolated chromophore where $r_{CI} = 1.59$ Å.

Further key CI seam features can be inferred from Figure 4. First, *no* CI exists for values of $z < 0.21$, since the degeneracy condition cannot be satisfied. Second, for increasing values of z, the intersection point is shifted to smaller r values. Finally, the FC geometry, whose (r, z) projection is indicated in the figure, is seen to lie at a certain distance from the CI seam. From a dynamical perspective, motion both in r and z will therefore be required to reach the seam region.

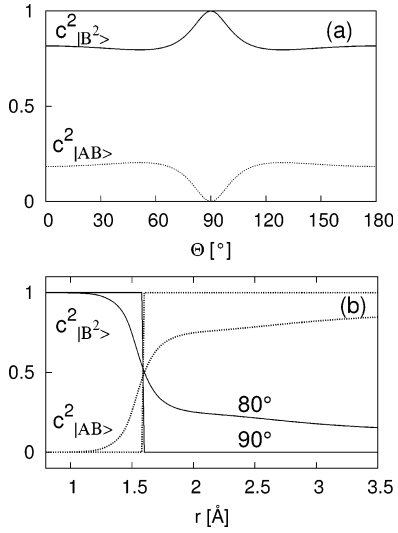

Figure 3. Decomposition of the eigenvector pertaining to the S_1 state in terms of its $|B^2\rangle$ and $|AB\rangle$ components, as a function of θ and r. Since the diabatic states are of VB type, i.e., have a fixed charge character (with the positive charge localized on the nitrogen end for $|AB\rangle$ and the positive charge localized on the hydrocarbon end for $|B^2\rangle$), the charge distributions for the adiabatic states can be directly inferred from the eigenvector decomposition. (a) S_1 eigenvector components as a function of the torsional angle θ, at $r = r_{CI} - \epsilon$, with $r_{CI} = 1.59$ Å. Full line: $|B^2\rangle$ component, dotted line: $|AB\rangle$ component. (b) Eigenvector components for the S_1 state as a function of the tuning coordinate r, at $\theta = 90°$ vs $\theta = 80°$. Full lines: $|B^2\rangle$ component, dotted lines: $|AB\rangle$ component. The figure illustrates the sudden change in charge character at $\theta = 90°$, which is smoothed out when moving away from the intersection point.

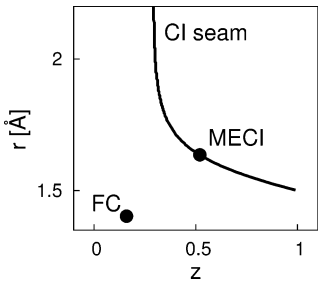

Figure 4. CI seam in the (r, z) plane ($\theta = 90°$), for the combined chromophore plus solvent system, comprising the coupling mode θ, tuning mode r, and the solvent coordinate z in the role of an additional tuning mode. The minimum energy CI is located at ($r_{min} = 1.54$ Å, $z_{min} = 0.55$). The (r, z) projection of the Franck−Condon geometry is shown for reference.

4.3. Frozen Solvent Limit. Figure 5 illustrates the adiabatic S_0 and S_1 surfaces as a function of r and θ, for two limiting situations: (i) an orientational solvent polarization equilibrated to the S_0 charge distribution at the Franck−Condon (FC) geometry ($r = r_{FC}$, $\theta = 0°$), with $z_0 = z_{FC,eq}^{S_0} = 0.16$, and (ii) a solvent polarization equilibrated to the S_1 charge distribution at the same geometry $z_0 = z_{FC,eq}^{S_1} = 0.84$. A related interpretation based upon solvent states equilibrated to the $|AB\rangle$ vs $|B^2\rangle$ diabatic states was given in ref 17.

With the logic detailed in ref 17, the equilibrium z values $z_{FC,eq}^{S_0}$ and $z_{FC,eq}^{S_1}$ are obtained from the minimum free energy

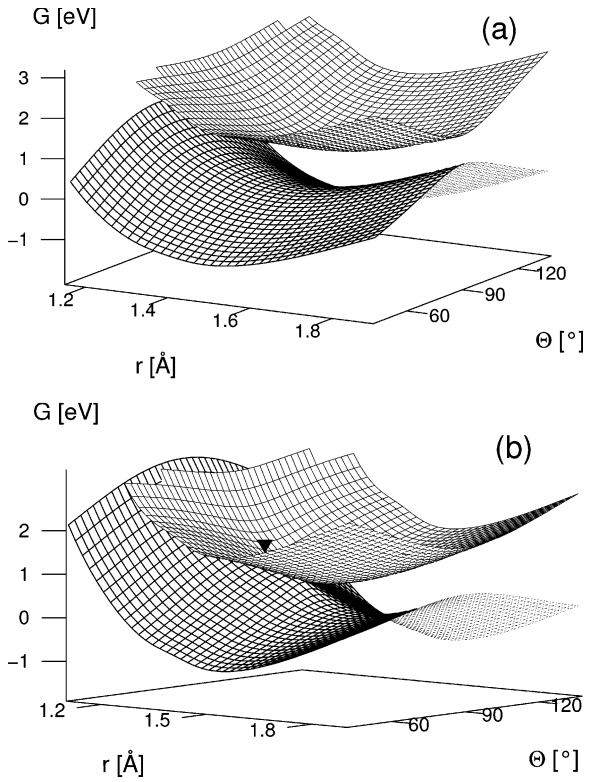

Figure 5. Free energy surfaces S_0 and S_1 for a frozen solvent situation (section 5.2.2), to be compared with Figure 1 for the isolated chromophore. Key: (a) solvent equilibrated to the S_0 charge distribution at the Franck−Condon geometry, $z_0 = z_{FC,eq}^{S_0} = 0.16$, where the CI has disappeared; (b) solvent equilibrated to the S_1 charge distribution at the same geometry, $z_0 = z_{FC,eq}^{S_1} = 0.84$, where the CI has been shifted to a smaller r value, $r_{CI} = 1.35$ Å (marked by a triangle).

condition

$$\left.\frac{\partial G_{S_0}(r,\theta,z)}{\partial z}\right|_{r=r_{FC},\theta=0^\circ} = k_s\,(z - c^{S_0}_{|B^2\rangle}(r,\theta,z))\Big|_{r=r_{FC},\theta=0^\circ} = 0 \tag{14}$$

for equilibrium solvation with respect to S_0, and a complementary expression for equilibrium solvation with respect to S_1. Hence, we have $z_{FC,eq}^{S_0} = c^{S_0}{}_{|B^2\rangle}{}^2$ (which is small), and $z_{FC,eq}^{S_1} = c^{S_1}{}_{|B^2\rangle}{}^2 = 1 - z_{FC,eq}^{S_0}$ (which is large) at the specified geometry.

The first situation (i) corresponds to a solvent which, upon photoexcitation, remains in an orientational polarization state adjusted to the S_0 charge distribution—in accordance with the FC principle—while the fast, electronic polarization instantaneously adapts to the S_1 charge distribution at the FC geometry. By contrast, in the second case (ii) the solvent is allowed to equilibrate to the S_1 charge distribution at the FC geometry, and is then assumed to be fixed in this orientational polarization state. For an ultrafast spectroscopic experiment, the first case (i) is the more appropriate zeroth-order picture.

In accordance with the above observations for the CI seam, the CI is lost for the case $z_0 = z_{FC,eq}^{S_0}$, and is shifted to smaller r values, $r < r_{CI}^0$, for $z_0 = z_{FC,eq}^{S_1}$ (with r_{CI}^0 the value for the isolated chromophore).[80] Concomitantly, the topology of the CI can change: While the CI is weakly *peaked* (close to the intermediate, or "semi-level" case of ref 81) in the absence of the solvent mode, the topology is weakly *sloped* with respect to r at $z_0 = z_{FC,eq}^{S_1}$. For an even larger value $z = 1$, the CI is sloped, and the minimum of the upper adiabatic (S_1) surface no longer coincides with the CI.[17,82]

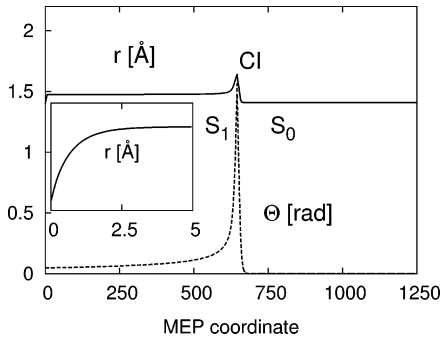

Figure 6. Minimum energy path for the isolated chromophore. For an S_1 initial condition at the Franck−Condon point ($r = 1.4$ Å, $\theta = 0°$), the figure shows the evolution of the (r, θ) components toward the CI point at ($r = r_{CI} = 1.59$ Å, $\theta = 90°$), and beyond this, the S_0 evolution toward the ground-state minimum. The inset shows the initial rapid increase in r, away from the FC point (see also Figure 1).

While the above considerations for particular z_0 values give a qualitatively correct picture, there is in reality always a *distribution* of z values about the z_0 value in question. If we consider again a FC transition, the initial equilibrium solvent distribution with respect to the ground state S_0 is transported to S_1, where it represents a nonequilibrium state. While the center z_0 of the distribution may not lie on the CI seam (as is the case for our model with $z_0 = z_{FC,eq}^{S_0}$), *part* of the overall distribution can in fact lie on the seam. In such a case, one would therefore have to take into account the possibility of some CI-induced excited-state decay even if the solvent were "frozen" in a state centered on z_0;[83] the remainder of the distribution would require solvent dynamics for such decay.

4.4. Minimum Energy Path Analysis. While a detailed understanding of the excited-state dynamics and the transition S_1-S_0 requires (quantum-)dynamical simulations, we discuss here certain features which can be derived from a minimum energy path (MEP) description including the solvent coordinate.[55,56] The MEP represents a mass-weighted steepest descent path; it is a generalization to the excited state[84] of solvent-coordinate dependent MEPs for ground-state reactions.[57−59,85] It is also a generalization of, e.g., the interpretation by Robb, Olivucci, and co-workers[18,30−32,34] for isolated chromophore excited-state CI problems to include a solvent coordinate.

Despite its limitations, important information can be deduced from the MEP description, notably on (i) whether the excited-state dynamics is characterized by barriers, (ii) whether the free energy regions accessed by the MEP lie in the vicinity of nonadiabatic coupling regions and whether the free energy minimum to which the MEP converges coincides with a MECI, (iii) what are the patterns of charge evolution along the MEP, and (iv) what are the solvent coordinate effects for the MEP approach to the CI seam.

In the following, we first give a brief discussion of the MEP for the isolated chromophore and then consider the combined solute−solvent system, with initial conditions as addressed in the preceding section.

4.4.1. MEP for Isolated Chromophore. For reference, Figure 6 illustrates the MEP for the isolated chromophore, starting from an S_1 initial condition in the FC region. By its steepest descent nature, the MEP leads to the global minimum of the S_1 surface, which here coincides with the CI point, and is continued from there to the S_0 surface.

With the mass $m_r = 6$ g mol^{-1} for the tuning coordinate r (skeletal stretch, or BLA coordinate) and the moment of inertia $I_\theta = 3.4$ g Å^2 mol^{-1} for the torsion (estimated from the torsional barrier height of about 45 kcal/mol at $\theta = 0°$ and a torsional

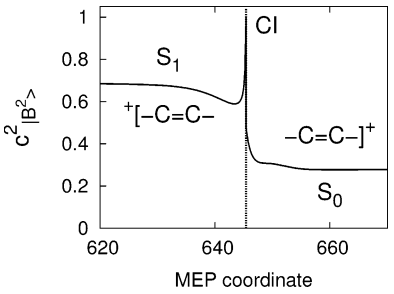

Figure 7. Eigenvector decomposition along the MEP (zoom on the vicinity of the CI). The squared $|B^2\rangle$ eigenvector coefficient reflects the evolution of the charge distribution along the S_1 vs S_0 portions of the MEP. At the CI point, a polarization effect is observed, such that $c^2_{|B^2\rangle} = 1$. The figure illustrates the net charge transfer $S_1 \rightarrow S_0$.

frequency of 560 cm^{-1};[33,86] see also ref 24), the very initial r motion is more rapid than that in θ. Given that the S_1 surface is locally bonding in θ, motion in r is indeed the very initial motion away from the FC point. In Figure 6, this is reflected in an almost instantaneous initial increase from $r = r_0 = 1.40$ Å to $r \simeq 1.48$ Å. The torsional angle θ initially increases slowly, and then follows an accelerating movement toward the CI point ($\theta = 90°$). By its continuation beyond the CI onto the S_0 surface, the MEP will subsequently reach the S_0 minimum geometry, corresponding to the solvent equilibrated to the cis or trans product.

Of particular interest is the overall evolution of the charge distribution, which follows three stages, as illustrated in Figure 7: (i) adiabatic S_1 charge distribution in the FC region, with predominant $|B^2\rangle$ character, (ii) polarization of the charge distribution toward an *exclusive* $|B^2\rangle$ component in the immediate vicinity of the CI (for $r < r_{CI}$), and (iii) evolution toward the S_0 minimum (cis or trans equilibrium), predominantly of $|AB\rangle$ character. The net effect of the S_1-S_0 transition is thus a shift of the positive charge from the carbon moiety—which was produced in the initial $S_0 \rightarrow S_1$ transition—to the nitrogen-containing end.

4.4.2. MEP for the Combined Solute−Solvent System. We now examine the S_1 MEP for the combined chromophore-solvent system, for two model solvents: (i) a very light solvent of mass $m_z = 7.68$ g Å^2 mol^{-1}, i.e., about $^1/_{46}$ the mass of acetonitrile (see also ref 24), and (ii) a heavy solvent of mass $m_z = 922$ g Å^2 mol^{-1}, i.e., about 2.6 times the mass of acetonitrile (whose mass is $m_z = 353$ g Å^2 mol^{-1}, for reference[8]). The solvent mass is determined as described in Appendix D. The solvent force constant k_s (here, $k_s = 2.5$ eV, see Table 1) is assumed to remain unchanged.

The global minimum free energy of the S_1 surface now corresponds to the MECI point, i.e., the minimum energy point along the CI seam. (This is a feature of our model; the MECI does not necessarily coincide with the global S_1 minimum.) The details of the MEP evolution toward the MECI depend on the relative (r,θ, z) time scales and, in particular, on whether the solvent is "slow" or "fast" as compared with the time scale set by the torsional motion.

We focus again on the initial conditions described above: First, a solvent orientational polarization $z_0 = z^{S_0}_{FC,eq}$, i.e., the *non*equilibrium initial condition resulting from the FC $S_0 \rightarrow S_1$ transition (Figure 8); second, a solvent polarization which is initially equilibrated to the S_1 charge distribution at the FC geometry, $z_0 = z^{S_1}_{FC,eq}$ (Figure 9). The solvent states along the MEP generally correspond to nonequilibrium polarization situations—unless the orientational solvent polarization is extremely fast and adjusts adiabatically rapidly to the S_1 charge

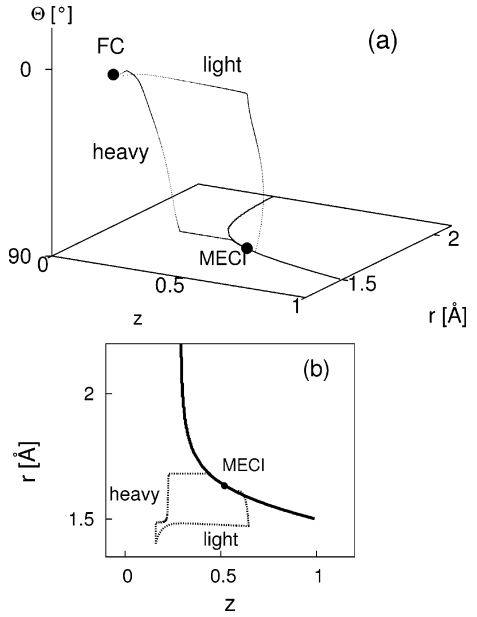

Figure 8. MEP evolution for the combined chromophore-solvent system, for a "light" model solvent vs a "heavy" model solvent, for the initial condition ($r = r_{FC}, \theta = 0°$, $z = z^{S_0}_{FC,eq}$). The evolution in the three-dimensional (r,θ, z) space (panel a) is shown, along with a projection onto the $(r, z)_{\theta = 90°}$ plane (panel b). The Franck−Condon (FC) point and minimum energy CI (MECI) points are marked.

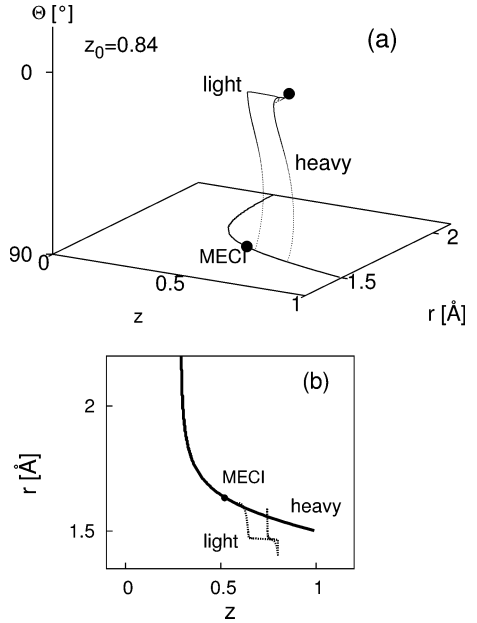

Figure 9. MEP evolution for the initial condition $z_0 = z^{S_1}_{FC,eq} = 0.84$. Analogously to Figure 8, the figure shows the evolution of the MEP in the three-dimensional (r,θ, z) space (panel a), along with a projection onto the $(r, z)_{\theta=90°}$ plane (panel b). In this case, the initial condition is compatible with the existence of a CI, so that the CI seam can be reached with little motion in z. (For a detailed discussion, see section 5.3.)

distribution as a function of the (r,θ) geometry. This latter case corresponds to the equilibrium solvation limit, as further discussed in refs 17 and 24.

The initial condition $z_0 = z^{S_0}_{FC,eq}$ reflects the fact that the solvent remains frozen—i.e., adjusted to the ground-state charge distribution—in the $S_0 \rightarrow S_1$ transition. This picture is best adapted to describe experimental situations involving a quasi-instantaneous laser excitation, as in the femtosecond laser experiments reported, e.g., in refs 37−39. As pointed out in

section 4.3, the CI is lost in this case, as a result of the "detuning" due to the energetically highly unfavorable nonequilibrium solvation situation. The subsequent events reflect the tendency of the solvent to adjust to the prevailing S_1 charge distribution (and the pronounced change in dipole moment accompanying the FC transition),[78] subject to the constraints imposed by the S_1 surface topology and the joint evolution with the internal degrees of freedom. Within the MEP description, the evolution tends toward the CI seam and ultimately toward the MECI.[87]

Figure 8 depicts the evolution of the MEP in the three-dimensional (r,θ, z) space (panel a), along with a projection onto the $(r, z)_{\theta=90°}$ plane (panel b). The CI seam of Figure 4 is shown for reference. The main features of the MEP evolution can be summarized as follows: (i) Depending upon the relative solvent and torsional time scales, the MECI is reached either via (r,θ, z) configurations away from the $(r, z)_{\theta = 90°}$ plane (light solvent case), or mainly via motion in the $(r, z)_{\theta=90°}$ plane after torsional motion $\theta = 0° \rightarrow \theta = 90°$ (heavy solvent case). (ii) Once the $(r, z)_{\theta=90°}$ plane is reached, the motion toward the MECI depends on the relative time scales of the two tuning modes z and r. Notice that the path toward the MECI in part *evolves along the CI seam*. (See also the Supporting Information for further illustration.)

A general feature of the two MEPs is that the CI seam is reached in the sequence corresponding to the time scales of the coordinates in the order: first, the fastest, second, the next fastest, and third, the slowest. It is interesting to observe that this is the opposite sequence for reaching a transition state in an activated chemical reaction (see e.g. refs 8 and 9). This reversal is due to the feature that motion toward the CI seam involves a descent, rather than an ascent, in free energy.

These aspects are further illustrated in Figure 9, for the $z_0 = z_{FC,eq}^{S_1}$ initial condition. Here, the solvent is initially equilibrated to the S_1 charge distribution and therefore exerts no pronounced "detuning" effect; in particular, a S_1/S_0 degeneracy exists for this solvent state. The CI seam can therefore be reached without motion in the solvent coordinate z, solely following motion in θ and r toward the location $r_{seam}(z_{FC,eq}^{S_1}) = 1.4$ Å. This pathway can indeed be identified for the heavy solvent case, as illustrated in Figure 9. Here, the seam is first reached with little motion in z, followed by a second portion of the MEP proceeding from the initial location on the seam to the MECI. Clearly, the seam itself represents a steepest descent path toward the MECI. Note that a discontinuity tends to occur in the gradient of the MEP when the CI seam is met. By contrast, the light solvent case entails that the minimum energy CI is essentially reached via (r,θ, z) configurations unrelated to the CI seam.

The present discussion has focused on the CI seam as the key topological feature, and has not addressed the actual nonadiabatic transitions $S_1 \rightarrow S_0$. In particular, the MEP evolution along the CI seam is a feature which is not generally representative of the actual dynamics. In an approximate dynamical perspective, nonadiabatic transitions would occur as soon as the CI seam is approached—independent of whether one is close to the MECI. Preliminary results of quantum dynamical and mixed quantum-classical simulations giving accurate information on the time-dependent state populations are reported in refs 23 and 24.

5. Conclusions and Outlook

The present work details and extends the analysis of ref 17 to describe the influence of an environment on a CI for situations where electrostatic interactions are dominant, such that the orientational polarization field of the environment interacts strongly with the chromophore, here illustrated for the S_1/S_0 CI in protonated Schiff bases. The combined chromophore-environment system is described by coupled free energy surfaces which include the internal molecular coordinates and a solvent coordinate.

Our perspective includes the solvent as an additional "tuning" mode which modulates the energy gap and displaces the CI from its vacuum value, generating a CI seam. The solvent's impact can be substantial: For example, if the solvent is initially equilibrated to the solute in its electronic ground state, and remains "frozen" following a FC transition, the CI can be entirely lost. In other situations, the topology may be altered (e.g., from "peaked" to "sloped"). Furthermore, the solvent can have off-diagonal contributions—solvent-induced couplings—which can have a symmetry-breaking effect at geometries (here, $\theta = 90°$) where the coupling intrinsic to the chromophore vanishes. Thus, the solvent's dynamics are expected to play a key role in, e.g., the pathway to the CI seam. We have addressed here aspects of the pathway from the Franck−Condon region to the CI seam in terms of a minimum energy path (MEP) description, which provides some qualitative conclusions on the potential dynamical pathways.

Forthcoming work will report on the relation between the MEP calculations and a detailed dynamical perspective. Preliminary results obtained by quantum-dynamical simulations[23] as well as approximate surface hopping calculations[24] have addressed the evolution in the chromophore's internal coordinates coupled to an inertial, nondissipative solvent dynamics. Work in progress includes frictional effects acting on both the solvent and the internal coordinates, an essential ingredient in allowing the highly excited chromophore to dissipate energy into the high-dimensional solvent environment.[88]

While the present level of discussion is approximate in a number of respects, and specifically for the PSB model studied here, several features are worth noting and are expected to carry over to a more complete description. In particular, (i) a charge polarization effect is expected to accompany the isomerization process in the PSBs, due to the decoupling of the diabatic states—$|AB\rangle$ and $|B^2\rangle$ in our model—at the 90° twisted geometry. This effect is related to previous observations by Robb, Olivucci and co-workers based on ab initio studies for several short retinal analogues.[18,32] Furthermore, (ii) the charge character of the adiabatic surfaces in the vicinity of the CI is strongly geometry dependent, as a result of the involvement of diabatic states corresponding to different charge distribution patterns. A similar feature has been pointed out in ref 35. With respect to both of the above aspects, explicit dynamical calculations will be required to account for the observable effects in the dynamics.

The dielectric continuum model considered here is the simplest realization of a description incorporating the relevant electrostatic interactions. It is suitable to describe the interaction with a polar and polarizable solvent, even though it is approximate even in this context. The model demonstrates the essential features of our approach: (i) The representation for the electronic states of the chromophore is specifically adapted to the chromophore-environment interaction. Since we focus on electrostatic interactions, a diabatic basis is chosen such as to exhibit a well-defined charge character. The two-electron two-orbital model employed naturally yields a VB type representation and thus provides a simple example of an appropriate basis. Future work will develop general strategies to formulate suitable diabatic basis representations. (ii) The free energy description augments the chromophore electronic structure problem with

the relevant features of the system-environment interaction. Importantly, the molecular level interactions can be recast in terms of such free energies, leading to the definition of generalized, microscopic solvent coordinates.[85,89−93] This paves the way for the application of the present approach to complex environments. The longer term goal is a solvent coordinate type description adapted to the local environment in highly specific environments like proteins. A formulation involving a Poisson−Boltzmann approach[94] is currently under development. (iii) The formulation in terms of nonequilibrium free energies, in conjunction with a kinetic energy associated with the orientational polarization or solvent coordinate(s), opens up the possibility of a dynamical description including the solvent, with a combined dynamical path for the chromophore-environment supermolecular system.

Further development of the above aspects, beyond the simple model proposed here, will be required for a detailed discussion of the dynamics in chromophores like the PSBs, PYP, and GFP. When combined with an ab initio based parametrization including all relevant modes of the chromophore, the present approach should contribute to clarifying various aspects of the environment's impact on the subpicosecond and picosecond dynamics in these systems. These developments are complementary to, and will be guided by the results of recent QM/MM calculations which address the microscopic details of the concerted chromophore-protein motions.[13,49]

Acknowledgment. This work was supported in part by a CNRS/DFG collaboration project and by NSF grants CHE-0108314 and CHE-0417570. We thank Lorenz Cederbaum, Riccardo Spezia, Todd Martínez, Evgeniy Gromov, and Monique Martin for valuable discussions.

Appendix A: Diabatic Model Potentials

As detailed in ref 17, the diagonal contributions of the diabatic potential eq 10 take the following form (here cited for the $|AB\rangle$ contribution)

$$V_{AB}(r,\theta) = V^{AB}_{morse}(r) + V^{AB}_{shift}(r,\theta) + V^{AB}_{\theta}(\theta) \quad (A.1)$$

with (i) a Morse form in the stretch coordinate r,

$$V^{AB}_{morse}(r) = D_{AB}\,(1 - \exp[-\alpha_{AB}\,(r - r_{0,AB})])^2 \quad (A.2)$$

where $r_{0,AB}$ is the C=C equilibrium distance at the planar geometry, (ii) a θ-dependent shift term which displaces the minimum of the Morse potential for increasing θ

$$V^{AB}_{shift}(r,\theta) = \xi_{AB}(r)\,\sin^2\theta \quad (A.3)$$

and (iii) a diagonal angle-dependent term chosen according to the study by Tennyson and Murrell for ethylene[66]

$$V^{AB}_{\theta}(\theta) = c^{AB}_{\theta}\,\cos^2\theta \quad (A.4)$$

with $c_\theta < 0$ such that the diabatic ground-state potential is bonding for $\theta = 0°$, see ref 66. Here, $\xi_{AB}(r) = c^{AB}_{shift}\,(r - r_{0,AB})\,\exp(-|r - r_{0,AB}|/\sigma_r)$ with $c^{AB}_{shift} = -2D_{AB}\alpha_{AB}{}^2\Delta r_{AB}$, for a shift Δr_{AB} in the minimum geometry. Note the exponential which is added to attenuate the effect of the linear term for increasing distance from the minimum geometry.

Similarly, the diagonal potential for the hole−pair state $|B^2\rangle$ is given as

$$V_{B^2}(r,\theta) = V^{B^2}_{morse}(r) + V^{B^2}_{shift}(r,\theta) + V^{B^2}_{\theta}(\theta) + V_{FC}(r,\theta) + \Delta E_{B^2} \quad (A.5)$$

with definitions analogous to eqs A.2−A.4, in addition to the Franck−Condon correction $V_{FC}(r,\theta)$ of eq 12 and an energy shift ΔE_{B^2} with respect to the $|AB\rangle$ state. Finally, the diabatic coupling is given in eq 11.

Appendix B. Definition of the Branching Space Vectors for the CI Model

A key concept in characterizing CIs is the so-called branching space,[81] defined by the principal directions along which the degeneracy at the CI is lifted. In the adiabatic picture, this space is spanned by the **h** (nonadiabatic coupling) and **g** (gradient difference) vectors

$$\mathbf{h} = \langle \Phi^{ad}_1 | \nabla H_{el} | \Phi^{ad}_2 \rangle$$
$$2\mathbf{g} = \langle \Phi^{ad}_1 | \nabla H_{el} | \Phi^{ad}_1 \rangle - \langle \Phi^{ad}_2 | \nabla H_{el} | \Phi^{ad}_2 \rangle \quad (B.1)$$

Here, we address the question of the contribution of the diabatic tuning and coupling modes—and, in particular, the contribution of the solvent coordinate—to these basic adiabatic quantities. In ref 95, Martínez and co-workers conjectured that the solvent mainly contributes to the **g** vector (and in this sense exerts a tuning effect in the adiabatic picture).

For the purpose of the present discussion, which entails a *local* analysis about the CI geometry, eq 2 is linearized with respect to r and θ,

$$\mathbf{G}(r,\tilde\theta,z) = \mathbf{V}_{CI}{}^{(0)}(r,\tilde\theta) + \frac{1}{2}k_s z^2 + \frac{1}{2}k_s\left(\frac{1}{2} - z\right) + \begin{pmatrix} \kappa^{(1)}\,r + \frac{1}{2}k_s\left(\frac{1}{2} - z\right) & \gamma\,\tilde\theta \\ \gamma\tilde\theta & \kappa^{(2)}\,r - \frac{1}{2}k_s\left(\frac{1}{2} - z\right) \end{pmatrix} \quad (B.2)$$

with $\tilde\theta = \theta - 90°$, and the linear coupling coefficients $\kappa^{(1,2)}$ determined so as to agree with the free energy eq 2 close to the CI. The form eq 2 corresponds to the so-called linear vibronic coupling model detailed, e.g., in ref 1.

We aim to express the adiabatic (**g**,**h**) quantities in terms of the diabatic parameters of eq 2. By introducing the diabatic-adiabatic transformation for the wave function, and following the analysis of ref 79, the following expressions for the adiabatic quantities are obtained,

$$\mathbf{g} = \begin{pmatrix} \Delta\kappa \\ \frac{1}{2}k_s \\ -\gamma \end{pmatrix} \qquad \mathbf{h} = \begin{pmatrix} \Delta\kappa \\ \frac{1}{2}k_s \\ \gamma \end{pmatrix} \quad (B.3)$$

with $\Delta\kappa = \kappa^{(1)} - \kappa^{(2)}$. Hence, the tuning and coupling modes contribute equally to *both* the **g** and **h** vectors. (This is a particular feature of symmetry-allowed CIs.[79])

Note, though, that the branching space vectors as defined in eq B.3 are not orthogonal. Following Yarkony,[3,4] one may *orthogonalize* the **g** and **h** vectors by the transformation

$$\bar{\mathbf{g}} = \mathbf{g}\cos 2\beta + \mathbf{h}\sin 2\beta$$
$$\bar{\mathbf{h}} = \mathbf{h}\cos 2\beta - \mathbf{g}\sin 2\beta \quad (B.4)$$

with

$$\tan 4\beta = \frac{2\,\mathbf{g}\cdot\mathbf{h}}{|\mathbf{h}|^2 - |\mathbf{g}|^2} \tag{B.5}$$

such that $\tan 4\beta = \infty$ in our case. Hence, $2\beta = \pi/2$ and $\cos 2\beta = \sin 2\beta = 1/\sqrt{2}$. The orthogonalized gradient vectors thus read

$$\bar{\mathbf{g}} = \frac{1}{\sqrt{2}}\begin{pmatrix} 2\Delta\kappa \\ k_s \\ 0 \end{pmatrix} \qquad \bar{\mathbf{h}} = \frac{1}{\sqrt{2}}\begin{pmatrix} 0 \\ 0 \\ 2\gamma \end{pmatrix} \tag{B.6}$$

By imposing orthogonality, we have obtained a $\bar{\mathbf{g}}$ vector that only comprises tuning mode contributions and an $\mathbf{h}$ vector that comprises only a coupling mode contribution. The solvent contribution is *entirely in the orthogonalized* $\bar{\mathbf{g}}$ *vector*, due to the fact that it was entirely of tuning type in the model eq 2. In this sense, our model is in agreement with the conclusions of ref 95.

Appendix C. Location of MECI

This Appendix addresses the location of the MECI, i.e., the minimum energy CI along the CI seam. The relevant condition is the one for a degeneracy of the two free energy states, so that the adiabatic solutions coincide,

$$G_{CI}(r_{CI}, z_{CI}) = \frac{1}{2}\left[G_{AB}(r,z,\theta) + G_{B^2}(r,z,\theta)\right]\Big|_{r=r_{CI},z=z_{CI},\theta=\pi/2} = \frac{1}{2}\left[V_{AB}(r,\theta) + V_{B^2}(r,\theta) + \frac{1}{2}k_s z^2 + \frac{1}{2}k_s (1-z)^2\right]\Big|_{r=r_{CI},z=z_{CI},\theta=\pi/2} \tag{C.1}$$

The free energy G_{CI} is a function of $(r = r_{CI}, z = z_{CI})$ along the seam. Because of the seam condition, only one of the two coordinates (r_{CI}, z_{CI}) is an independent variable. To identify the minimum free energy along the seam, we can therefore consider the derivative, e.g., with respect to the solvent coordinate,

$$\frac{dG_{CI}}{dz_{CI}} = \frac{\partial G_{CI}}{\partial z_{CI}} + \frac{\partial G_{CI}}{\partial r_{CI}}\frac{\partial r_{CI}}{\partial z_{CI}} = 0 \tag{C.2}$$

This translates to

$$k_s\, z_{CI} - k_s\,(1 - z_{CI}) + \frac{\partial G_{CI}}{\partial r_{CI}}\frac{\partial r_{CI}}{\partial z_{CI}} = 0$$

$$k_s\,(2z_{CI} - 1) + \frac{\partial G_{CI}}{\partial r_{CI}}\frac{\partial r_{CI}}{\partial z_{CI}} = 0 \tag{C.3}$$

The first term by itself would yield the result $z_{CI} = 0.5$; to this adds the partial derivative $(\partial r_{CI}/\partial z_{CI})$. The difference between the actual MECI—for our model, at $z_{CI} = 0.55$—and the value 0.5 is accounted for by this additional term (as confirmed numerically).

Appendix D. Dynamical Solvent Description and Solvent Mass

While the free energy functional $G[\psi_{el}, \mathbf{P}_{el}, \mathbf{P}_{or}]$ addresses the energetics of the solute−solvent system, the dynamics of the combined system hinges upon the introduction of a kinetic energy for the orientational polarization field[55,56,96−100]

$$K_{or} = \frac{1}{2}m_s \int d\mathbf{x}\,[\dot{\mathbf{P}}_{or}(\mathbf{x})]^2 \tag{D.1}$$

The orientational polarization mass has been defined, in polaron theory, as $m_s = (1/\omega_s^2)\,4\pi/(1 - \epsilon_\infty/\epsilon)$, with the solvent frequency ω_s.[101,100]

With the definition eq 1 of the nonequilibrium polarization field, the kinetic energy K_{or} takes the form[99]

$$K_{or} = \frac{1}{2}m_s \int d\mathbf{x}\left[\dot{z}(\mathbf{P}^{eq}_{or,B^2} - \mathbf{P}^{eq}_{or,AB}) + z\left(\frac{\partial \mathbf{P}^{eq}_{or,B^2}}{\partial \mathbf{R}} - \frac{\partial \mathbf{P}^{eq}_{or,AB}}{\partial \mathbf{R}}\right)\dot{\mathbf{R}}\right]^2 \tag{D.2}$$

Note the dependence on the internal coordinates $\mathbf{R}$ that arises as a consequence of the dependence of the equilibrium polarization $\mathbf{P}^{eq}_{or}$ on $\mathbf{R}$. The resulting kinetic energy couplings may necessitate redefining the solvent coordinate such as to obtain a diagonal form of K_{or}.[99,7] However, in the present first discussion, we do not perform this redefinition and ignore any issues of kinetic energy coupling associated with the solvent.

In practice, the solvent frequency ω_s can be obtained[102,84] from experimental measurements of the short-time, inertial solvation dynamics.[103,104] The solvent mass can then be determined from the solvent frequency and the force constant, $m_s = k_s/\omega_s^2$.[84]

Supporting Information Available: Text giving a study of the solvation perspective and minimum energy path and figures showing free energy cuts along the solvent coordinate z, free energy cuts along the tuning coordinate r, and minimum energy paths. This material is available free of charge via the Internet at http://pubs.acs.org.

References and Notes

(1) Köppel, H.; Domcke, W.; Cederbaum, L. S. *Adv. Chem. Phys.* **1984**, *57*, 59.
(2) Domcke, W.; Stock, G. *Adv. Chem. Phys.* **1997**, *100*, 1.
(3) Yarkony, D. R. *Rev. Mod. Phys.* **1996**, *68*, 985.
(4) Yarkony, D. R. *J. Phys. Chem.* **1996**, *100*, 18612.
(5) Klessinger, M.; Michl, J. *Excited States and Photochemistry of Organic Molecules*, VCH: New York, 1995.
(6) Michl, J.; Bonačić-Koutecký, V. *Electronic Aspects of Organic Photochemistry*; Wiley: New York, 1990.
(7) Laage, D.; Burghardt, I.; Sommerfeld, T.; Hynes, J. T. *Chem. Phys. Chem.* **2003**, *4*, 61.
(8) Laage, D.; Burghardt, I.; Sommerfeld, T.; Hynes, J. T. *J. Phys. Chem. A* **2003**, *107*, 11271.
(9) Burghardt, I.; Laage, D.; Hynes, J. T. *J. Phys. Chem. A* **2003**, *107*, 11292.
(10) Toniolo, A.; Granucci, G.; Martínez, T. J. *J. Phys. Chem. A* **2003**, *107*, 3822.
(11) Hayashi, S.; Tajkhorshid, E.; Schulten, K. *Biophys. J.* **2003**, *85*, 1440.
(12) Groenhof, G.; Bouxin-Cademartory, M.; Hess, B.; de Visser, S. P.; Berendsen, H. J. C.; Olivucci, M.; Mark, A. E.; Robb, M. A. *J. Am. Chem. Soc.* **2004**, *126*, 4228.
(13) Andruniów, T.; Ferré, N.; Olivucci, M. *Proc. Natl. Acad. Sci. U.S.A.* **2004**, *101*, 17908.
(14) Yamazaki, S.; Kato, S. *J. Chem. Phys.* **2005**, *123*, 114510.
(15) Kühl, A.; Domcke, W. *J. Chem. Phys.* **2002**, *116*, 263.
(16) Cederbaum, L. S.; Gindensperger, E.; Burghardt, I. *Phys. Rev. Lett.* **2005**, *94*, 113003.
(17) Burghardt, I.; Cederbaum, L. S.; Hynes, J. T. *Faraday Discuss. Chem. Soc.* **2004**, *127*, 395.
(18) Garavelli, M.; Celani, P.; Bernardi, F.; Robb, M. A.; Olivucci, M. *J. Am. Chem. Soc.* **1997**, *119*, 6891.
(19) Ben-Nun, M.; Molnar, F.; Lu, H.; Phillips, J. C.; Martínez, T. J.; Schulten, K. *Faraday Discuss. Chem. Soc.* **1998**, *110*, 447.
(20) Hahn, S.; Stock, G. *J. Phys. Chem. B* **2000**, *104*, 1146.
(21) Worth, G. A.; Meyer, H.-D.; Cederbaum, L. S. *J. Chem. Phys.* **1998**, *109*, 3518.
(22) Ferretti, A.; Granucci, G.; Lami, A.; Persico, M.; Villani, G. *J. Chem. Phys.* **1996**, *104*, 5517.
(23) Burghardt, I.; Cederbaum, L. S.; Hynes, J. T. *Comput. Phys. Comm.* **2005**, *169*, 95.
(24) Spezia, R.; Burghardt, I.; Hynes, J. T. *Mol. Phys.* **2006**, *104*, 903.

(25) Bonačić-Koutecký, V.; Koutecký, J.; Michl, J. *Angew. Chem., Int. Ed. Engl.* **1987**, *26*, 170.
(26) Song, L.; El-Sayed, M. A.; Lanyi, J. K. *Science* **1993**, *261*, 891.
(27) Nonella, M.; *J. Phys. Chem. B* **2000**, *104*, 11379.
(28) Heyne, K.; Herbst, J.; Dominguez-Herradon, B.; Alexiev, U.; Diller, R. *J. Phys. Chem.* **2000**, *104*, 6053.
(29) Toniolo, A.; Olsen, S.; Manohar, L.; Martínez, T. J. *Faraday Discuss. Chem. Soc.* **2004**, *127*, 149.
(30) Vreven, T.; Bernardi, F.; Garavelli, M.; Olivucci, M.; Robb, M. A.; Schlegel, H. B. *J. Am. Chem. Soc.* **1997**, *119*, 12687.
(31) Garavelli, M.; Vreven, T.; Celani, P.; Bernardi, F.; Robb, M. A.; Olivucci, M. *J. Am. Chem. Soc.* **1998**, *120*, 1285.
(32) González-Luque, R.; Garavelli, M.; Bernardi, F.; Merchán, M.; Robb, M. A.; Olivucci, M. *Proc. Natl. Acad. Sci. U.S.A.* **2000**, *97*, 9379.
(33) Garavelli, M.; Negri, F.; Olivucci, M. *J. Am. Chem. Soc.* **1999**, *121*, 1023.
(34) Garavelli, M.; Bernardi, F.; Robb, M. A.; Olivucci, M. *J. Mol. Struct. (THEOCHEM)* **1999**, *463*, 59.
(35) Molnar, F.; Ben-Nun, M.; Martínez, T. J.; Schulten, K. *J. Mol. Struct. (THEOCHEM)* **2000**, *506*, 169.
(36) Ben-Nun, M.; Molnar, F.; Schulten, K.; Martínez, T. J. *Proc. Natl. Acad. Sci. U.S.A.* **2002**, *99*, 1769.
(37) Schoenlein, R. W.; Peteanu, L. A.; Mathies, R. A.; Shank, C. V. *Science* **1991**, *254*, 412.
(38) Schoenlein, R. W.; Peteanu, L. A.; Mathies, R. A.; Shank, C. V. *Science* **1994**, *266*, 422.
(39) Gai, F.; Hasson, K. C.; McDonald, J. C.; Anfinrud, P. A. *Science* **1998**, *279*, 1886.
(40) Genick, U. K.; Soltis, S. M.; Kuhn, P.; Canestrelli, I. L.; Getzoff, E. D. *Nature (London)* **1998**, *392*, 206.
(41) Mataga, N.; Chosrowjan, H.; Taniguchi, S.; Hamada, N.; Tokunaga, F.; Imamoto, Y.; Kataoka, M. *Phys. Chem. Chem. Phys.* **2003**, *5*, 2454.
(42) Kandori, H.; Katsuta, Y.; Ito, M.; Sasabe, H. *J. Am. Chem. Soc.* **1995**, *117*, 2669.
(43) Logunov, S. L.; Song, L.; El-Sayed, M. A. *J. Phys. Chem.* **1996**, *100*, 18586.
(44) Changenet, P.; Plaza, P.; Martin, M. M. *Chem. Phys. Lett.* **2001**, *336*, 439.
(45) Changenet-Barret, P.; Espagne, A.; Katsonis, N.; Charier, S.; Baudin, J. B.; Jullien, L.; Plaza, P.; Martin, M. M. *Chem. Phys. Lett.* **2002**, *365*, 285.
(46) Zgrablić, G.; Voïtchovsky, K.; Kindermann, M.; Haake, S.; Chergui, M. *Biophys. J.* **2005**, *88*, 2779.
(47) In addition, the isomerization quantum yield for retinal is much higher in the protein environment (65% as compared with 20% in solution phase[105]) and the bond selectivity is very pronounced, in contrast to the unspecific isomerization in a solvent.
(48) Bonačić-Koutecký, V.; Schöffel, K.; Michl, J. *Theor. Chim. Acta* **1987**, *72*, 459.
(49) Rohrig, U. F.; Guidoni, L.; Laio, A.; Frank, I.; Rothlisberger, U. *J. Am. Chem. Soc.* **2004**, *126*, 15328.
(50) Ruiz, D. S.; Cembran, A.; Garavelli, M.; Olivucci, M.; Fuss, W. *Photochem. Photobiol.* **2002**, *76*, 622.
(51) Bonačić-Koutecký, V.; Köhler, J.; Michl, J. *Chem. Phys. Lett.* **1984**, *104*, 440.
(52) Worth, G. A.; Cederbaum, L. S. *Chem. Phys. Lett.* **2001**, *338*, 219.
(53) Worth, G. A.; Cederbaum, L. S. *Chem. Phys. Lett.* **2001**, *348*, 477.
(54) Note that the solvent polarization is composed of a slow orientational component and a fast electronic component, $\mathbf{P}(\mathbf{x}) = \mathbf{P}_{el}(\mathbf{x}) + \mathbf{P}_{or}(\mathbf{x})$. The present treatment does not address the electronic component explicitly; the latter is assumed to adjust adiabatically rapidly, in a Born−Oppenheimer type picture.[61]
(55) Lee, S.; Hynes, J. T. *J. Chem. Phys.* **1988**, *88*, 6853.
(56) Lee, S.; Hynes, J. T. *J. Chem. Phys.* **1988**, *88*, 6863.
(57) Gertner, B. J.; Ando, K.; Bianco, R.; Hynes, J. T. *Chem. Phys.* **1994**, *183*, 309.
(58) Bianco, R.; i Timoneda, J. J.; Hynes, J. T. *J. Phys. Chem.* A **1994**, *98*, 21103.
(59) Mathis, J. R.; Kim, H. J.; Hynes, J. T. *J. Am. Chem. Soc.* **1993**, *115*, 8248.
(60) A similar solvent coordinate was originally introduced for electron-transfer reactions not involving such nuclear motion or bond breaking.[96,100]
(61) Kim, H. J.; Hynes, J. T. *J. Chem. Phys.* **1992**, *96*, 5088.
(62) Ando, K.; *J. Chem. Phys.* **1997**, *107*, 4585.
(63) Hahn, S.; Stock, G. *Chem. Phys.* **2000**, *259*, 297.
(64) Here, "critical" refers to the critical value of the asymmetry parameter δ (cf. eq 6), which leads to an S_1-S_0 degeneracy, while "heterosymmetric"—as opposed to homosymmetric and nonsymmetric[25]—indicates that the orbitals localized on neighboring centers have different energies.
(65) The triplet $^3|AB\rangle$ state is not involved in the processes considered here.
(66) Tennyson, J.; Murrell, J. N. *Nouv. J. Chim.* **1981**, *5*, 361.
(67) Bonačić-Koutecký, V.; Bruckmann, P.; Hiberty, P.; Koutecký, J.; Leforestier, C.; Salem, L. *Angew. Chem., Int. Ed. Engl.* **1975**, *14*, 575.
(68) Krawczyk, P.; Viel, A.; Manthe, U.; Domcke, W. *J. Chem. Phys.* **2003**, *119*, 1397.
(69) Brooks, B. R.; Schaefer, H. F., III. *J. Am. Chem. Soc.* **1979**, *101*, 307.
(70) As a parenthetical remark, note the relation of the perturbations of the first type to the "sudden polarization" effect for twisted, pyramidalized ethylene.[5,6,25,66,67,68,107,108] Here, the term "polarization" again refers to the strong mixing of the states $|Z_+\rangle$ and $|Z_-\rangle$, and hence, their polarization towards the $|A^2\rangle$ and $|B^2\rangle$ components, here induced by a one-sided pyramidalization. The case of ethylene is particular in that the $|Z_+\rangle$ and $|Z_-\rangle$ states are almost degenerate at the 90° twisted geometry, and only a weak perturbation is required to "polarize" these states.[25] Ethylene therefore belongs to the "weakly heterosymmetric" class of ref 25. By contrast, the parameter δ takes large values for the PSBs.
(71) Cembran, A.; Bernardi, F.; Olivucci, M.; Garavelli, M. *Proc. Natl. Acad. Sci. U.S.A.* **2005**, *102*, 6255.
(72) Note that a more flexible choice of the diabatic basis—in particular, a basis defined so as to feature well-defined charge properties in the nonadiabatic coupling region while simultaneously coinciding with the adiabatic states at the planar geometry—would entail less restrictions on the validity of the two-state model eq 10.
(73) Beyond the two-mode description, other internal modes may play a nonnegligible role. In particular, Martínez and co-workers[35] have pointed out that the CN stretch is of importance at the CI geometry in a retinal analog,[35] and is possibly predominant as compared with the skeletal stretch.[109] In the shortest Schiff bases like formaldimine,[110] evidence for the key role of the pyramidalization mode has been provided. While the present analysis is restricted to a two-mode model, the model can be readily extended to account for these additional modes.
(74) Laage, D.; Thompson, W. H.; Blanchard-Desce, M.; Hynes, J. T. *J. Phys. Chem.* A **2003**, *107*, 6032.
(75) Thompson, J.; Bashford, D.; Noodleman, L.; Getzoff, E. D. *J. Am. Chem. Soc.* **2003**, *125*, 8186.
(76) Weiss, R. M.; Warshel, A. *J. Am. Chem. Soc.* **1979**, *101*, 6131.
(77) Reference 68 further introduces an r dependence in the coupling which is not taken into account at the present level of the analysis.
(78) This change has been reported to be about 12 D for retinal[111−113] and even 26 D for the coumaric acid chromophore of PYP.[114]
(79) Köppel, H. *Faraday Discuss. Chem. Soc.* **2004**, *127*, 35.
(80) The shift in the CI location entails a corresponding shift in the charge distribution patterns as described in the previous section: Due to the role of the solvent as an additional tuning mode, the pattern of Figures 6−8 is shifted in r but not changed.
(81) Atchity, J.; Xantheas, S. S.; Ruedenberg, K. *J. Chem. Phys.* **1991**, *95*, 1862.
(82) Related considerations on the role of CI topology have been addressed in refs 36 and 95.
(83) For further discussion of these aspects, see ref 115.
(84) Kim, H. J.; Hynes, J. T. *J. Photochem. Photobiol.: Chemistry* **1997**, *105*, 337.
(85) Benjamin, I.; Barbara, P. F.; Gertner, B. J.; Hynes, J. T. *J. Phys. Chem.* **1995**, *99*, 7557.
(86) Ayala, P. Y.; Schlegel, H. B. *J. Chem. Phys.* **1998**, *108*, 2314.
(87) In a more complete dynamical description, the motion of the joint solute−solvent distribution would include oscillatory features which are not captured by the MEP.[23,24]
(88) As has been shown previously in the context of ground-state reactions,[55,56,99,116,84,7] generalized dissipation—i.e., time-dependent frictional effects within a Langevin treatment—needs to be incorporated to fully account for the solvent impact on the reactive process.
(89) Ando, K.; Hynes, J. T. *J. Phys. Chem.* **1997**, *101*, 10464.
(90) Warshel, A.; Weiss, R. M. *J. Am. Chem. Soc.* **1980**, *102*, 6218.
(91) Kierstead, W. P.; Wilson, K. R.; Hynes, J. T. *J. Chem. Phys.* **1995**, *95*, 5256.
(92) Warshel, A.; Chu, Z. T. *J. Phys. Chem. B* **2001**, *105*, 9857.
(93) Warshel, A.; Chu, Z. T.; Hwang, J.-K. *Chem. Phys.* **1991**, *158*, 303.
(94) Honig, B.; Nicholls, A. *Science* **1995**, *268*, 1144.
(95) Toniolo, A.; Ben-Nun, M.; Martínez, T. J. *J. Phys. Chem. A* **2002**, *106*, 4679.
(96) Marcus, R. A. *J. Chem. Phys.* **1956**, *24*, 966.
(97) Calef, D. F.; Wolynes, P. G. *J. Phys. Chem.* **1983**, *87*, 3387.
(98) Hynes, J. T. *J. Phys. Chem.* **1986**, *90*, 3701.
(99) Borgis, D.; Hynes, J. T. *Chem. Phys.* **1993**, *170*, 315.
(100) Ulstrup, J.; *Charge-transfer processes in condensed media*; Springer: Berlin, 1979.
(101) Fröhlich, H. *Adv. Phys.* **1954**, *3*, 325.
(102) Carter, E. A.; Hynes, J. T. *J. Chem. Phys.* **1991**, *94*, 5961.
(103) Maroncelli, M. *J. Mol. Liq.* **1993**, *57*, 1.
(104) Horng, M. L.; Gardecki, J. A.; Papazyan, A.; Maroncelli, M. *J. Phys. Chem.* **1995**, *99*, 17311.

(105) Becker, R. S.; Freedman, K. *J. Am. Chem. Soc.* **1985**, *107*, 1477.
(106) Experimental results comparing different solvent environments do not give evidence, though, for a pronounced influence of the solvent viscosity and polarity on the short-time dynamics.[43,46] These findings contradict the expectation that the electrostatic solvent properties should play an important role. The model developed in the present manuscript should contribute to clarifying these issues.
(107) Ohmine, I.; *J. Chem. Phys.* **1985**, *83*, 2348.
(108) Mestdagh, J. M.; Visticot, J. P.; Elhanine, M.; Soep, B. *J. Chem. Phys.* **2000**, *113*, 237.
(109) This change is observed to be smooth at $\theta = 90°$, in contrast to the sudden, step function-like change depicted in Figure 3b.[35] However, as shown in Figure 5b, a slight offset from $\theta = 90°$ can also imply a smooth behavior. Note further that ref 35 associates the **g** vector with a predominant contribution from the CN stretch mode, and only a minor contribution from the CC stretch.
(110) Doltsinis, N. L.; Marx, D. *Phys. Rev. Lett.* **2002**, *88*, 166402.
(111) Schenkl, S.; van Mourik, F.; van der Zwan, G.; Haacke, S.; Chergui, M. *Science* **2005**, *309*, 917.
(112) Huang, J.; Chen, Z.; Lewis, A. *J. Phys. Chem.* **1989**, *93*, 3314.
(113) Mathies, R.; Stryer, L. *Proc. Natl. Acad. Sci. U.S.A.* **1976**, *73*, 2169.
(114) Premvardhan, L. L.; van der Horst, M. A.; Hellingwerf, K. J.; van Grondelle, R. *Biophys. J.* **2003**, *84*, 3226.
(115) Non-Adiabatic Effects in Chemical Dynamics, General Discussion. *Faraday Discuss.* **2004**, *127*, 447.
(116) Fonseca, T.; Kim, H. J.; Hynes, J. T. *J. Mol. Liq.* **1994**, *60*, 161.